RECENT ADVANCES IN NANOPARTICLE-INCORPORATED DIAMOND-LIKE CARBON FILMS

F.R. Marciano[a,b*], D.A. Lima-Oliveira[a], R.S. Pessoa[b], E.C. Almeida[a], N.S. Da-Silva[c], E.J. Corat[a,b] and V.J. Trava-Airoldi[a,b]

[a] *Instituto Nacional de Pesquisas Espaciais (INPE), Laboratório Associado de Sensores e Materiais (LAS), Av. dos Astronautas 1758, São José dos Campos, 12227-010, SP, Brazil.*
[b] *Instituto Tecnológico de Aeronáutica (ITA), Centro Técnico Aeroespacial (CTA), Pça. Marechal Eduardo Gomes, 50 - São José dos Campos, 12228-900, SP, Brazil.*
[c] *Universidade do Vale do Paraíba (Univap), Instituto de Pesquisas e Desenvolvimento (IP&D), Laboratório de Biologia Celular e Tecidual, Av. Shishima Hifumi, 2911 - São José dos Campos, 12244-000, SP, Brazil.*

*Corresponding author: Fernanda Roberta Marciano
Tel.: +55 12-3945-6576
Fax: +55 12-3945-6717
E-mail: **fernanda@las.inpe.br**

Abstract

Diamond-like Carbon (DLC) films have been the focus of extensive research in recent years due to its potential application as surface coatings. Silver (Ag), crystalline diamond (NCD) and titanium dioxide (TiO_2) in the form or nanoparticles were incorporated in DLC films for different applications. The films were growth on 316L stainless steel substrates from a dispersion of these nanoparticles in hexane using plasma enhanced chemical vapor deposition. The presence of SNP increases the DLC wear resistance against oxygen etching. NCD particles reduced the steel pitting corrosion, improving DLC and stainless steel electrochemical corrosion resistance and preventing aggressive ions from attacking metallic surfaces. TiO_2 nanoparticles increased DLC bactericidal activity. In addition, TiO_2–DLC films increase the chemical interaction between bacteria and the films, which is an additional factor for the increasing bactericidal activity. From these results, nanoparticle-incorporated DLC films increase the range of applications of these coatings, adding them new properties.

Keywords: diamond-like carbon, silver, crystalline diamond, titanium dioxide, nanoparticles, hexane.

1. Introduction

Diamond-like carbon (DLC) films have been actively studied over the last decade in the field of material engineering. Consisting of dense amorphous carbon or hydrocarbon, DLC mechanical properties fall between those of graphite and diamond, which means these films present low friction coefficient and high hardness (Robertson, 2002; Donnet et al, 2002; Yun et al, 2008). Due to their mechanical, electrical, optical and chemical properties, the use of DLC coatings in mechanical and electrical fields has increased with recent applications in food, beverage and medical market segments (Donnet et al, 1997).

Metal ions incorporated into solid films in a controlled way are very important for academic research and industrial applications (Schmid, 1992; Wang et al, 1988). Metal ion-doped solid films can acquire different properties that can combine the properties of the metal ion particles, especially if they are nanoparticles, and the bulk of the host material (Shirakura et al, 2006; Ohno et al, 1997; Matsumoto et al, 1981; Tanaka et al, 1996; Takahara et al, 2001). In the case of DLC films, the main reported problem in producing these films is the difficulty of dispersing particles homogeneously in the DLC matrix (Schiffmann et al, 1999; Hussain et al, 2006).

A new technique developed in our laboratory permits the deposit of DLC films from hexane (Marciano et al, 2009a). With this technique, it is possible to deposit films from a dispersion of different kind of nanoparticles in hexane in order to create different kind of DLC films for different applications. In this paper, we show the main results obtained in our laboratories from the production and characterization of nanoparticle-incorporated DLC films.

2. Experimental procedures

Silicon (100) and 316L stainless steel were used as substrates. The stainless steel were polished by using up 0.25 μm diamond powder and cleaned ultrasonically in an acetone bath for 15 min before putting them into the vacuum chamber. All the substrates were cleaned ultrasonically in an acetone bath for 15 min, and then dried in nitrogen atmosphere. The clean samples were mounted on a water-cooled, 10-cm diameter cathode into the plasma chamber.

The cathode was fed by a pulsed DC power supply, with variable pulse voltage from -100 to -1000V, at a frequency of 20 kHz and duty-cycle of 50 %.

In the chamber (vacuum base pressure of 1.3 mPa) the substrates were additionally cleaned by argon discharge with 1 sccm gas flow at 11.3 Pa working pressure and a discharge voltage of -700 V for 10 min prior to deposition. In order to enhance the DLC film adhesion to metallic surfaces, a thin amorphous silicon interlayer (thickness around 200 nm) were deposited using silane as the precursor gas (1 sccm gas flow at 11.3 Pa for 12 min and a discharge voltage of -700 V) (Bonetti et al, 2006). The DLC films were deposited using hexane as the feed gas to a thickness of around 2.0 μm (at 18.0 Pa for 60 min and a discharge voltage of -700 V).

To produce the nanoparticle-incorporated DLC films, different kind of nanoparticles were dispersed in hexane at different proportions. These dispersions replaced the pure hexane during the DLC deposition.

3. Results and discussion

Some results of the production and characterization of nanoparticle-incorporated DLC films according to the applications are as follows.

3.1. Anti-etching properties

Spacecraft surfaces in the Low Earth Orbit (LEO), with altitudes of 200-600 Km, suffer the bombardment with atomic oxygen, which is the dominant atmospheric element in LEO (Tagawa et al, 1990). Exterior coatings used in large space structures are necessary and endurance tests against the atomic oxygen bombardments of the uncoated parts such as solid lubricants are needed (Tagawa et al, 1990). In this area, DLC films as a solid lubricant coating represent an important area of investigation related to space devices.

Silver nanoparticles (SNP) have received considerable attention due to their attractive physical and chemical properties (Sileikaite et al, 2006). SNP with ~60nm of average particle size were incorporated into DLC films in order to reduce the oxygen plasma etching. To produce Ag-DLC films, SNP dispersion in hexane at 1.0, 5.0 and 10.0 g/L, replaced the pure hexane during the deposition.

Figure 1 shows the morphology of SNP in an Ag-DLC film produced from a dispersion of 5.0 g/L of SNP in hexane. Figure 1a shows the scanning electron microscopy (SEM) image acquired by using a field emission gun scanning electron microscopy (FEG-SEM), JEOL JSM-6330F, with 30.0 kV, and Fig. 1b shows the atomic force microscopy (AFM) image acquired by using the dynamic tip mode of a VEECO Multimode V AFM.

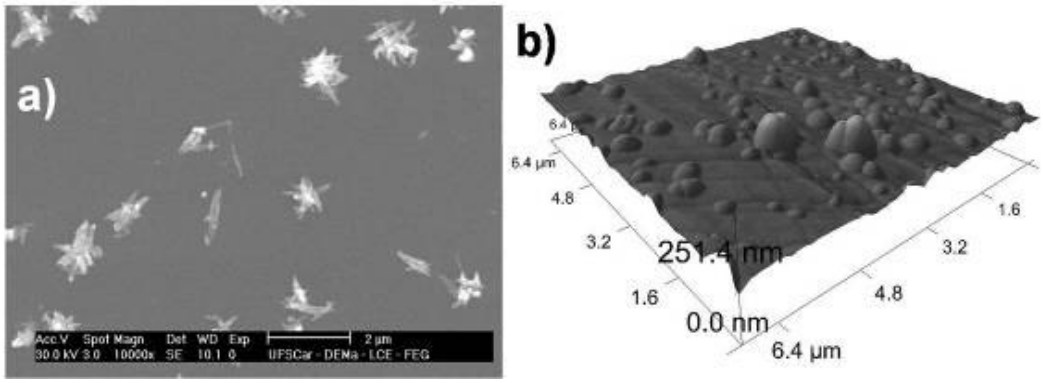

Figure 1. (a) SEM and (b) AFM images of an Ag-DLC film produced from a dispersion of 5.0 g/L of SNP in hexane.

As illustrated in Fig. 1, it was possible to reach a satisfactory density of nanoparticles with the adopted methodology. The images reveal that SNP are not dispersed absolutely homogeneous. One may observe that two or more nanoparticles may be representing a large particle. Figure 1b shows some nanoparticle completely immersed in DLC films and others partially immersed in DLC surface. SEM and AFM images show the tendency of the inter-particle distances became smaller with the increase in number density of particles culminating in some clusters coming closer to one another.

The etching of carbon-based materials, like DLC films, can be done with discharges operating at low-pressure oxygen plasma. To analyze DLC degradation in situ, etching experiments were performed in a reactive ion etching (RIE) reactor using O_2 as the etchant gas. The samples were partially covered with a mechanical mask to produce a step between the etched and non-etched regions. The profile of this step was analyzed by a prophilometer (Alpha-Step 500), and the etching rates were determined. The analysis of the relative concentration of species extracted from the plasma was performed by using a quadrupole mass spectrometer AccuQuad 200D, with resolution 1 amu, adapted to the vacuum chamber through a drifting tube. More details about the RIE system and this characterization methodology can be found in our previous publications (Marciano et al, 2008; Marciano et al, 2009b).

Figure 2 shows the obtained etching rates as function of SNP concentration in hexane dispersion. The etching shows that with an addition of 10.0 g/L of SNP in hexane, the etching rate suffers a decrease of more than 2 times of initial value, reaching a decrease of up to 3.5 times to a maximum hexane solution concentration of 10.0 g/L.

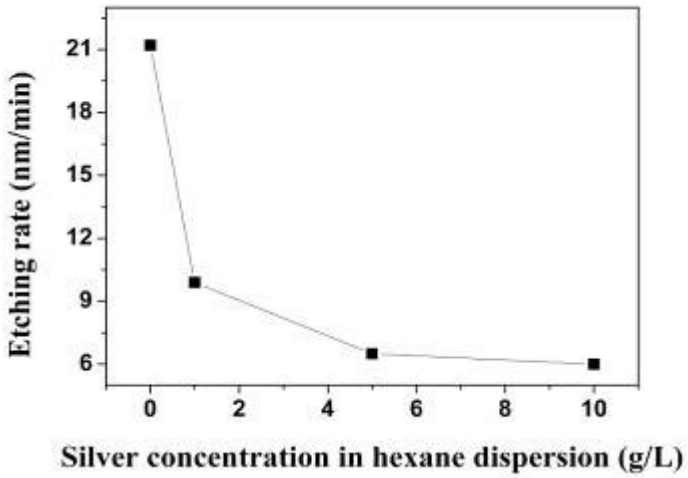

Figure 2. Etching rate as function of SNP concentration in hexane dispersion.

Also for this case, we have made the process monitoring by mass spectrometry, but with one difference, the main etching species CO^+ and CO_2^+ are monitored in real time at an interval range of 1 second between each detection. This permitted us to see how the signals of the species vary during all etching process, allowing a better evaluation of the effect of the silver concentration on the wear of the film. In Fig. 3, the time evolution of CO^+ and CO_2^+ species is presented during the oxygen plasma

degradation for DLC samples produced for (a) pure hexane, (b) 1.0 g/L SNP hexane dispersion, (c) 5.0 g/L SNP hexane dispersion and (b) 10.0 g/L SNP hexane dispersion. In this figure, on point 1, oxygen gas had started to be inserting in the chamber, point 2, plasma (10 W) had been on, and, point 3, plasma and oxygen had been off. We can see that when the discharge is on, a significant increase in the partial pressure of CO^+ and CO_2^+ species can be observed, indicating the reaction of oxygen species with the substrate material. After the discharge ignition the signals tends to decrease rapidly with time indicating a constant decrease in etching rate. This fact shows to be more prominent for higher silver concentrations.

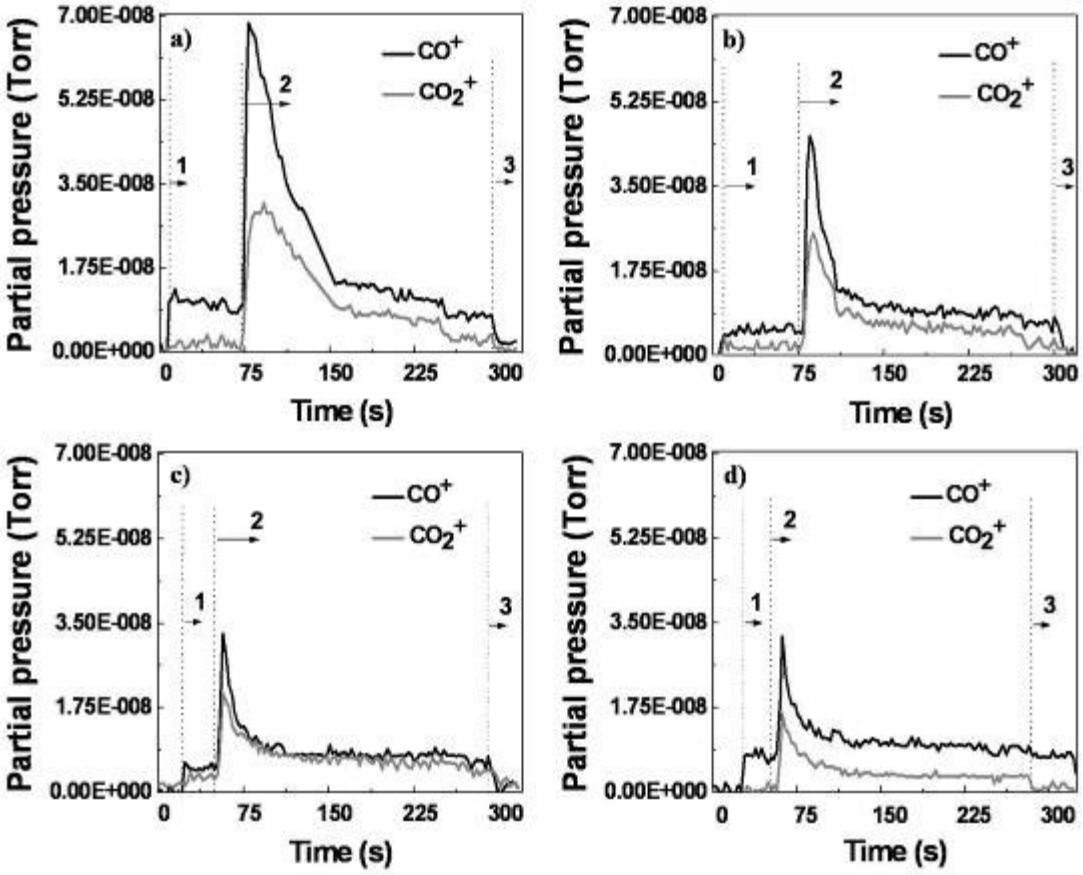

Figure 3. Temporal evolution of CO^+ e CO_2^+ species during the etching process of the DLC films produced from (a) pure hexane, (b) 1.0 g/L SNP hexane dispersion, (c) 5.0 g/L SNP hexane dispersion, and (d) 10.0 g/L SNP hexane dispersion. On point 1, oxygen gas had started to be inserting in the chamber, point 2, plasma (10 W) had been on, and, point 3, plasma and oxygen had been off.

It is known from the literature, that the etching process of the DLC material by cold plasmas is performed with the use of oxygen gas (Lieberman et al, 2005). This, due

to reaction with carbon, promotes the generation of volatile products CO and CO_2 that are pumped out by the vacuum system. With the insertion of SNP in the film volume, the etching process of the film becomes slower, since silver has a higher reaction affinity with oxygen atoms forming a silver oxide layer on DLC surface owing to the irradiation of oxygen plasma. Oxygen atoms react preferentially with silver preventing the reaction of oxygen with carbon from the DLC films. The result of this experiment can be seen in Fig. 2, where the obtained etching rate decreases with the increase of SNP in DLC bulk. The increase of SNP in the film proved to be very efficient in reducing the reaction of oxygen with carbon. This result was also verified by the analysis of etching environment with mass spectrometer (see Fig. 3). The partial pressure of CO^+ and CO_2^+ showed a decreased with the increase of SNP, indicating that the film etching decreases with the increase of SNP.

3.2. Anti-corrosive properties

Another good property reported is the DLC electrochemical corrosion resistance (Wang et al, 2008; Sharma et al, 2008; Liu and Kwek, 2008). It is known DLC electrochemical corrosion behavior is heavily dependent on the film composition and structure, which are in turn depended on the deposition technique and precursor gas (Wang et al, 2008). Nanocrystalline diamond (NCD) particles with ~250 nm of average particle size were incorporated into DLC films in order to investigate NCD-DLC electrochemical corrosion resistance.

Electrochemical tests were performed using a conventional three-electrode electrochemical cell (Oliveira et al, 2003). In this cell, the reference electrode was a saturated Ag/AgCl electrode, the counter electrode was a platinum wire and the working electrodes were the stainless steel, DLC and NCD-DLC films. The electrolyte solution was a 0.5 mol/L sodium chloride (NaCl) aqueous solution, pH 5.8, which was not stirred and was naturally aerated. Potentiodynamic tests were carried out by polarization of samples in the anodic direction, from -2.0 to +2.0 V, just after exposition to the electrolyte solution. The potential sweep rate was 1 mV/s. The impedance measurements were also carried out in 0.5 mol/L NaCl aqueous solution, pH 5.8. The electrochemical impedance spectra (EIS) were obtained over the frequency range 100 kHz–10 mHz, at open circuit potential, with an AC excitation of 10 mV. All experiments were performed at room temperature. The electrochemical stability of the systems in the test solution was investigated by the open-circuit potentials (OCP). The greatest E_{corr} value of -0.321 mV was observed for NCD-DLC films. The negative OCP values for the samples may be caused by the penetration of the test solution (Liu et al, 2008; Kim et al, 2005). The electrochemical parameters obtained from the potentiodynamic polarization curves (Fig. 4) are given in Tab. 1. The corrosion current density (i_{corr}) of NCD-DLC films reduced by more than 5 times with comparison to the stainless steel. The protective efficiency (Kim et al, 2005) calculated from corrosion current density also indicates NCD-DLC films offer the best protection among the uncoated samples up to 81.3%. In general, samples in the corrosion behavior with lower current density and higher potential indicate better corrosion resistance (Manca et al, 1999). An improvement in the NCD-DLC corrosion

resistance is evidenced by a shift of the polarization curve towards the region of lower current density and higher potential. Even DLC films presented the best protective effect at high anodic potentials, with a greater tendency to passivate, the presence of nanoporous on its surface increase its corrosion current density.

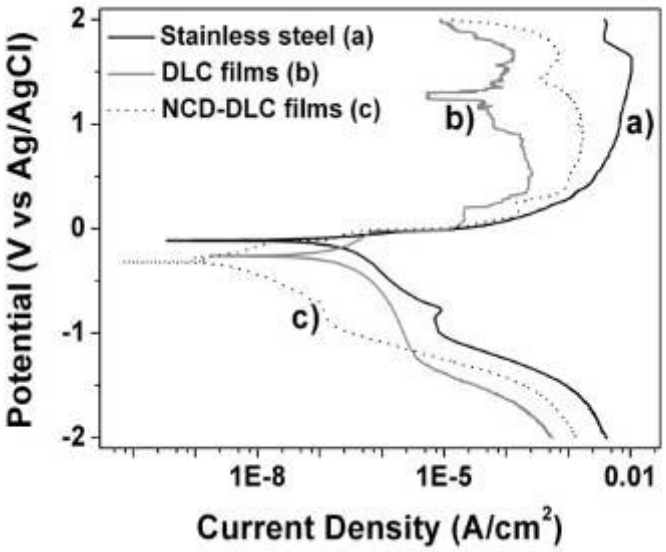

Figure 4. Potentiodynamic polarization curves of stainless steel, DLC and NCD-DLC films in NaCl at room temperature.

Table 1. Electrochemical parameters obtained from potentiodynamic polarization curves in NaCl at room temperature.

Samples	E_{corr} (mV)	i_{corr} (nA/cm^2)	Protective efficiency (%)
Stainless steel	-0.117	0.359	-
DLC films	-0.241	1.740	-748.8
NCD-DLC films	-0.321	0.067	81.3

The Nyquist plots determined by electrochemical impedance spectroscopy (EIS) in Fig. 5 show the different corrosion behavior of the samples after immersion in NaCl. NCD-DLC films present superior impedance in comparison to the pure DLC and the stainless steel. The enhancement in corrosion resistance of the NCD-DLC samples can be attributed to the reduced electrical conductivity caused by the intrinsic chemical inertness of the NCD-DLC films in comparison to the uncoated samples (Manca et al, 1999). In addition, NCD-DLC films can act as a passive film to prevent aggressive ions from attacking the substrate and thereby improve the corrosion resistance of 316L stainless steel (Fig. 6). The chloride (Cl^-) ions of the NaCl solution attack the protective oxide layer on 316 stainless steel surface, penetrating to the austenite matrix and resulting in pitting corrosion (Feng et al, 2003). The NCD-DLC samples show very little pitting corrosion. NCD particles may occupy the nanoporous in DLC films, preventing the attacking of the Cl^- ions.

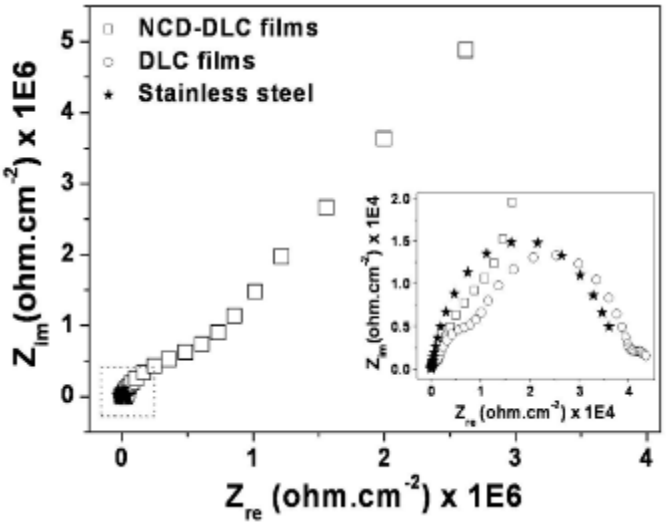

Figure 5. a) Nyquist plot of stainless steel, DLC and NCD-DLC films. b) Enlargement of the region within the rectangular box in (a).

The SEM images of NCD-DLC film after the electrochemical corrosion test (Fig. 6b) shows minor NCD particles that did not belong to the film surface (Fig. 6a). These NCD particles probably block the attacking of Cl^- ions, forming a barrier against the corrosion.

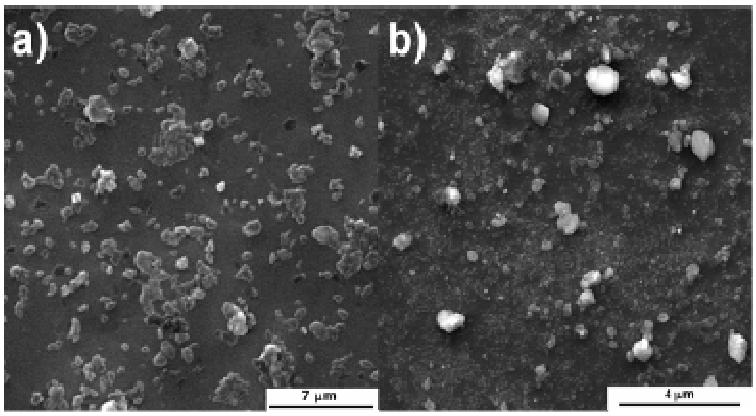

Figure 6. SEM images of NCD-DLC films (a) before and (b) after the electrochemical corrosion tests.

From the results here presented, it is possible to see NCD-DLC films improving DLC and stainless steel electrochemical corrosion resistance. NCD-DLC prevented aggressive ions from attacking metallic surfaces, becoming a potential candidate for an anti-corrosion material in industrial applications.

3.3. Antibacterial properties

Titanium dioxide (TiO_2) has been widely studied as regards various electronic applications, utilizing the photo-catalytic nature and transparent conductivity, which strongly depend on the crystalline structure, morphology and crystallite size (Nakano et al, 2009). Due to TiO_2 photo-semiconductor properties, it may find an application as antibacterial agent for the decomposition of organisms (Huang et al, 2000; Shun-Wen et al, 2008). TiO_2 in the anatase crystalline form is a strong bactericidal agent when exposed to near UV-light (Ireland et al, 2003).

TiO_2 nanoparticles with average particle size of 21 nm, in anatase crystalline form (Aeroxide® TiO2 P25 from Evonik) were dispersed in hexane at 0.1, 0.5 and 1.0 g/L. These dispersions replaced the pure hexane during the DLC deposition. The antibacterial activity of the TiO_2-DLC films was determined using *Escherichia coli* ATCC 25922 (*E. coli*, gram negative). More details about the antibacterial test methodology can be found in our previous publication (Marciano et al, 2009c).

Figure 7 shows the antibacterial activity of the stainless steel coated and non-coated with DLC and TiO_2-DLC films in different TiO_2 concentrations. The pure DLC films killed at about 32.5% of the total bacteria content. However, the bactericidal effect of TiO_2-DLC films was increasing with the increasing of TiO_2 content.

The exact killing mechanism(s) underlying the TiO_2 photocatalytic reaction is not yet well understood. Huang et al (2000) proposed a detailed mechanism for the bactericidal effect of TiO_2 photocatalytic reaction. They pointed out the initial oxidative damage takes place on the cell wall, where the TiO_2 photocatalytic surface makes first contact with intact cells. Cells with damaged cell wall are still viable. After eliminating the protection of the cell wall, the oxidative damage takes place on the underlying cytoplasmic membrane. Photocatalytic action progressively increases the cell permeability, and subsequently allows the free efflux of intracellular contents that eventually leads to cell death.

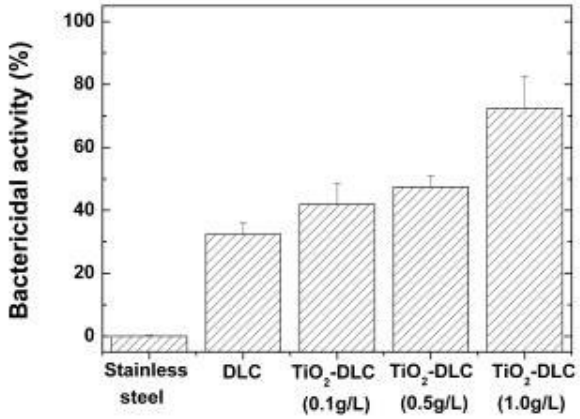

Figure 7. Antibacterial activity of the stainless steel coated and non-coated with DLC and TiO_2-DLC films in different TiO_2 concentrations.

Figure 8 shows SEM images of *E. coli* in direct contact with (a) stainless steel, (b) DLC, (c) 0.1g/L TiO_2-DLC, (d) 0.5g/L TiO_2-DLC and (e) 1.0g/L TiO_2-DLC films. All the images are in the amplification of 10,000x. The adhered bacterial citoplasmatic projections show the possible interaction between bacteria and the films.

The antibacterial activity of the pure DLC films was already been reported in previously publications (Marciano et al, 2008; Marciano et al, 2009d). Recent studies suggest that the physical interaction of carbon-based nanomaterials with bacteria is the primary killing mechanism (Ohno et al, 1997; Schiffmann et al, 1999; Wang et al, 2004). Carbon aggregates can cause irrecoverable damage to the studied bacteria by physical damage to the outer membrane of the cells, causing the release of intracellular content, as shown in Fig. 4b and 4g (Wang et al, 2004). On the images of TiO_2–DLC films, it is possible to see more bacterial citoplasmatic projections with the increase of TiO_2 nanoparticles in DLC films.

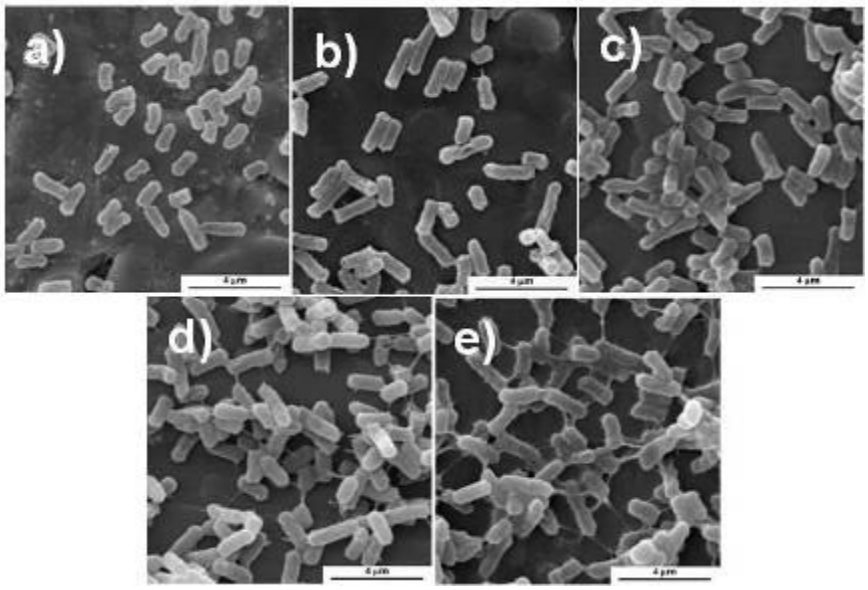

Figure 8. SEM images of *E. coli* in direct contact with (a) stainless steel, (b) DLC, (c) 0.1g/L TiO_2-DLC, (d) 0.5g/L TiO_2-DLC and (e) 1.0g/L TiO_2-DLC films. All the images are in the amplification of 10,000x.

According to Wang et al (2004), bacterial colonization on a surface is a complex process and the initial phase is bacterial adhesion to the biomaterial substrate. From a physicochemical point of view, the adhesion of bacteria cells to a surface is determined by the interplay of electrostatic and hydrophobic/hydrophilic interactions.

The interfacial free energy of adhesion (ΔF_{Adh}) for bacteria to attach the coatings was calculate according to Schneider, 1996. Table 2 presents the interfacial free energy of adhesion of the samples according to the concentration of TiO_2 nanoparticles in DLC films. The as-deposited DLC films presented ΔF_{Adh} = +17.6 mJ/m^2. According to the thermodynamic theory, the bacterial adhesion is unfavorable if the work of adhesion is

positive. The TiO_2-DLC films produced from 1.0 g/L TiO_2 in hexane presented ΔF_{Adh} = -5.2 mJ/m^2. In this case, the bacterial adhesion is favourable.

Table 2. Work of adhesion of the TiO_2-DLC samples according to the TiO_2 concentration in the films.

TiO_2 Concentration (g/L)	**Interfacial free energy of adhesion (mJ/m^2)**
0.0	17.6
0.1	1.8
0.5	-0.4
1.0	-5.2

Figure 9 compared the theoretical values of work of adhesion with the practical results of antibacterial activity. The good correlation coefficient (R^2 = 0.9999) shows that the bactericidal mechanism suffers influences not only from the presence of TiO_2 nanoparticles on the DLC surface, but also from the interaction between the nanoparticles and the DLC film, changing its proper characteristics.

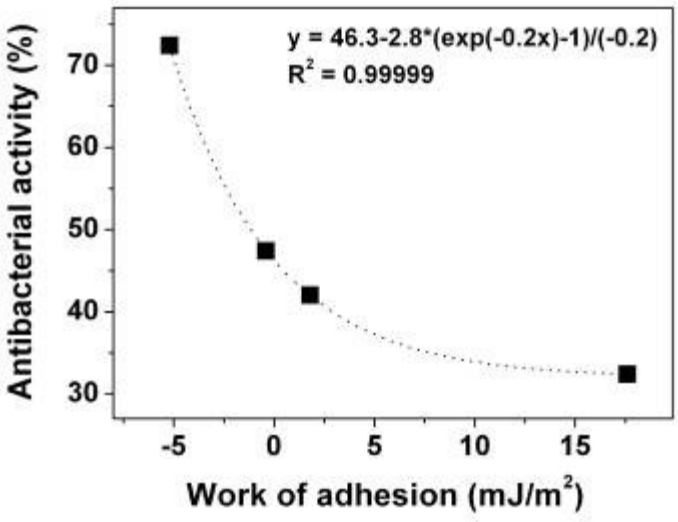

Figure 9. Antibacterial activity vs. work of adhesion.

These results suggest that as the TiO_2 content in DLC films increased, they become thermodynamically favorable to bacterial adhesion, increasing the direct contact between bacteria and more TiO_2 nanoparticles, promoting the increase in the bactericidal activity.

4. Conclusion

In this manuscript, it was reported the main results obtained in our laboratories from the production and characterization of nanoparticle-incorporated DLC films. The presence of SNP increases the DLC wear resistance against oxygen etching. The evolution of CO_2^+ and CO^+ due to oxygen ion attack decreases with the increase of SNP in DLC bulk. SNP react with oxygen at a high rate, becoming a sink to the oxygen species close to the DLC films surface.

NCD particles improve DLC and stainless steel electrochemical corrosion resistance. These particles reduced the pitting corrosion, which is an indication of the chemical inertness of the NCD-DLC coatings to the Cl^- ions. NCD-DLC films prevented aggressive ions from attacking metallic surfaces, becoming a potential candidate for an anti-corrosion material in industrial applications.

TiO_2 nanoparticles increased DLC antibacterial activity against *E. coli*. Thermodynamic approaches also show the increasing in bacterial adhesion with the increasing of TiO_2 content due to the increasing of interaction between bacteria and the studied films. TiO_2-DLC films can be useful in biomedical applications in general.

DLC films have a huge range of applications. As it was demonstrated in this manuscript, the nanoparticle-incorporated DLC films can modified the DLC structure increasing this range of applications with new scientific and technological applications.

As a final conclusion, it is so apparent that the Space Research area is very important not only for space area itself but, mainly, for giving direct and immediate contribution for health, petroleum, corrosion, mechanical, etc. areas.

Acknowledgements

This study was supported by Conselho Nacional de Desenvolvimento Científico e Tecnológico (CNPq) and Fundação de Amparo à Pesquisa do Estado de São Paulo (FAPESP).

References

Bonetti, L.F.; Capote, G.; Santos, L.V.; Corat, E.J.; Trava-Airoldi, V.J. *Thin Solid Films* 515 (2006) 375.

Donnet, C. ; Fontaine, J. ; Le Mogne, T. ; Belin, M. ; Héau, C. ; Terrat, J.P. ; Vaux, F.; Pont, G. *Surf. Coat. Technol.* 120 (1999) 548.

Feng, H.P.; Hsu, C.H.; Lu, J.K.; Shy, Y.H. *Mater. Sci. Eng. A* 347 (2003) 123.

Huang, Z.; Maness, P.C.; Blake, D.M.; Wolfrum, E.J.; Smolinski, S.L.; Jacoby, W.A. *J. Photochem. Photobiol. A. Chem.* 130 (2000) 163.

Hussain, S.; Roy, R.K.; Pal, A.K. *Mater. Chem. Phys.* 99 (2006) 375.

Ireland, J.C.; Klostermann, P.; Rice, E.W.; Clark, R.M. *Appl. Environ. Microbiol.* 59 (1993) 1668.

Kim, H.G.; Ahn, S.H.; Kim, J.G.; Park, S.J.; Lee, K.R. *Diamond Relat. Mater.* 14 (2005) 35.

Lieberman, M.A.; Lichtenberg, A.J. *Principles of Plasma Discharges and Materials Processing*; 0471720011; John Wiley & Sons: New York, NY, 2005; Vol. 1, 1-721.
Liu, E. ; Kwek, H.W. *Thin Solid Films* 516 (2008) 5201.
Liu, C.; Xu, M.; Zhang, W.; Pu, S.; Chu, P.K. *Diamond Relat. Mater.* 17 (2008) 1738.
Manca, J.V.; Nesladek, M.; Neelen, M.; Quaeyhaegens, C.; De Schepper, L.; De Ceuninck, W. *J. Microelectron Reliab.* 39 (1999) 269.
Marciano, F.R.; Bonetti, L.F.; Pessoa, R.S.; Marcuzzo, J.S.; Massi, M.; Santos, L.V.; Trava-Airoldi, V.J. *Diamond Relat. Mater.* 17 (2008) 1674.
Marciano, F.R.; Bonetti, L.F.; Da-Silva, N.S.; Corat, E.J.; Trava-Airoldi, V.J. *Synth. Met.* 159 (2009) 2167 (a).
Marciano, F.R.; Bonetti, L.F.; Pessoa, R.S.; Massi, M.; Santos, L.V.; Trava-Airoldi, V.J. *Thin Solid Films* 517 (2009) 5739 (b).
Marciano, F.R.; Lima-Oliveira, D.A.; Da-Silva, N.S.; Diniz, A.V.; Corat, E.J.; Trava-Airoldi, V.J. *J. Colloid Interf. Sci.* 340 (2009) 87 (c).
Marciano, F.R.; Bonetti, L.F.; Da-Silva, N.S.; Corat, E.J.; Trava-Airoldi, V.J. *J. Appl. Surf. Sci.* 255 (2009) 8377 (d).
Matsumoto, Y.; Kurimoto, J.; Shimizu, T.; Sato, E. *J. Electrochem. Soc.* 108 (1981) 1040.
Nakano, H.; Hasuike, H.; Kisoda, K.; Nishio, K.; Isshiki, T.; Harima, H. *J. Phys. Condens. Matter.* 21 (2009) 064214.
Ohno, T.; Haga, D.; Fujihara, K.; Kaiazaki, K.; Matsumura, M. J. *Phys. Chem. B* 101 (1997) 6415.
Oliveira, M.A.S.; Vieira, A.K.; Massi, M. *Diamond Relat. Mater.* 12 (2003) 2136.
Robertson, J. *Mat. Sci. Eng. R* 37 (2002) 129.
Schneider, R.P. *J. Colloid Interface Sci.* 182 (1996) 204.
Schiffmann, K.I.; Fryda, M.; Goerigk, G.; Lauer, R.; Hinze, P.; Bulack, A. *Thin Solid Films* 347 (1999) 60.
Schmid, G. *Chem. Rev.* 92 (1992) 1709.
Sharma, R.; Barhai, P.K.; Kumari, N. *Thin Solid Films* 516 (2008) 5397.
Shirakura, A.; Nakaya, M.; Koga, Y.; Kodama, H.; Hasebe, T.; Suzuki, T. *Thin Solid Films* 494 (2006) 84.
Shun-Wen, W.; Bing, P.; Li-Yuan, C.; Yun-Chao, L.; Zhu-Ying, L. *Trans. Nonferrous Met. Soc. China* 18 (2008) 1145.
Sileikaite, A.; Prosycevas, I.; Puiso, J.; Juraitis, A.; Guobiene, A. *Mater. Sci.* 12 (2006) 287.
Tagawa, M.; Ueno, M.; Ohmae, N. in: American Institute of Aeronautics and Astronautics, *28th Aerospace Sciences Meeting*, Reno, N.V., Jan 8-11, 1990, p. 728.
Takahara, Y.; Kondo, J.N.; Takata, T.; Lu, D.L.; Domen, K. *Chem. Mater.* 13 (2001) 1194.
Tanaka, T.; Takenaka, S.; Funabiki, T.; Yoshida, S. *J. Chem. Soc. Faraday Trans.* 92 (1996) 1975.
Wang, Q.F.; Yu, H.J.; Zhong, L.; Liu, J.Q.; Sun, J.Q.; Shen, J.C. *Chem. Mater.* 18 (2006) 1988.

Wang, J.; Huang, N.; Pan, C.J.; Kwok, S.C.H.; Yang, P.; Leng, Y.X.; Chen, J.Y.; Sun, H.; Wan, G.J.; Liu, Z.Y.; Chu, P.K. *Surf. Coat. Technol.* 186 (2004) 299.
Wang, Z. ; Wang, C. ; Wang, Q. ; Zhang, J. ; Zhang, J. *Appl. Surf. Sci.* 254 (2008) 3021.
Yun, D.Y.; Choi, W.S.; Park, Y.S.; Hong, B. *Appl. Surf. Sci.* 254 (2008) 7925.